

Spin Asymmetries in Squark and Gluino Production at Polarized Hadron Colliders

T. Gehrmann, D. Maître and D. Wyler

*Institut für Theoretische Physik, Universität Zürich, Winterthurerstrasse 190,
CH-8057 Zürich, Switzerland*

Abstract

We study the production cross sections for squarks and gluinos in collision of longitudinally polarized hadrons. The corresponding polarized partonic cross sections are computed in leading order supersymmetric QCD. The resulting asymmetries are evaluated for the polarized proton collider RHIC, as well as for hypothetical polarized options of the Tevatron and the LHC. These asymmetries turn out to be sizable over a wide range of supersymmetric particle masses. Once supersymmetric particles are discovered in unpolarized collisions, a measurement of the spin asymmetries would thus potentially help to establish the properties of the newly discovered particles and open a window to detailed sparticle spectroscopy at future polarized hadron colliders.

1 Introduction

Data from inclusive and semi-inclusive deep inelastic scattering off polarized targets [1–5] and from upcoming polarized proton-proton collisions at RHIC [6] continue to improve on our knowledge on the polarized parton distributions in the nucleon. They parametrise the probability of finding partons inside the nucleon having their spin aligned or anti-aligned to the nucleon spin and are obtained from a global fit [7–12] to spin asymmetries in polarized lepton-hadron and hadron-hadron collisions. They can be used to predict cross sections in collisions of hadrons with fixed spin orientation.

In the near future, one could therefore envisage to study polarized hadronic collisions not only to probe the structure of the colliding hadrons, but also to employ the polarization information in searches for new physics beyond the standard model. So far, there is very little theoretical work in this direction. The only comprehensive studies of new physics searches in polarized hadronic collisions to date concern the effects of contact interactions [13, 14] and of new gauge bosons [15] on spin asymmetries at RHIC and HERA. It was found that polarization information can yield vital insights, such as discriminating different types of contact interactions that yield identical signatures at unpolarized colliders. Likewise, one would expect that the additional information would strongly improve the study of other new physics scenarios.

Probably the most promising scenarios for physics beyond the standard model is its supersymmetric extension, formulated in the minimal supersymmetric standard model (MSSM) [16]. The effects of beam polarization in supersymmetric particle production have been studied in detail [17, 18] for a future linear electron-positron collider [19]. In the same context, fermion pair production in polarized photon-photon collisions [20] and gluino pair production in polarized electron-positron and polarized direct photon-photon collisions have been examined [21]. In all these studies, it was demonstrated that beam polarization asymmetries could be helpful in determining several parameters of the MSSM [22].

Spin asymmetries in supersymmetric particle production at hadron colliders have so far been considered in early studies addressing particular partonic production channels for squark and gluino production [23] and scalar lepton production [24].

On the other hand, the production of squarks and gluinos at hadron colliders is a QCD process and depends only on the squark and gluino masses, thus allowing a precise prediction [25] independent of other parameters of the MSSM. The expected cross sections for present and future hadron colliders turn out to be sizable and are further enhanced by QCD next-to-leading order corrections [26]. Non-observation of squark and gluino signatures at the Tevatron thus turns into stringent limits on the squark and gluino masses in the framework of the MSSM [27]: $m_{\tilde{q}} > 250$ GeV, $m_{\tilde{g}} > 195$ GeV.

These limits are substantially weakened if more complicated supersymmetric models than the MSSM are considered. In such non-minimal realizations of supersymmetry, squark and gluino production is also mediated by QCD interactions, thus yielding the same production cross sections as in the MSSM. Unfortunately, the non-standard decay modes of squarks and gluinos in these models cannot be distinguished from background processes at unpolarized colliders. One such model was for example advocated to explain an apparent excess in the bottom production cross section at the Tevatron [28], predicting gluino and squark masses as low as several GeV.¹

In the present paper, we calculate the spin asymmetries in squark and gluino production at polarized hadron colliders. At present, there is only RHIC at BNL where two polarized proton beams with a maximum centre-of-mass energy of $\sqrt{s} = 500$ GeV collide. Obviously, this is not sufficient to produce the MSSM sparticles; however they could be within reach if supersymmetry is realized in a more exotic scenario. To illustrate the potential of a future polarized hadron collider with a centre-of-mass energy comparable to Tevatron or LHC, we also study the anticipated spin asymmetries at polarized versions of Tevatron and LHC. Up to now, beam polarization has not been considered as a realistic upgrade option for these colliders, in part because the physics potential of such an option was not studied. With this paper we also wish to direct attention to this possibility.

The paper is organised as follows. In Section 2, we derive the spin-dependent parton level cross sections for squark and gluino production at hadron colliders in leading order QCD. Section 3 contains numerical

¹Data from electron-positron annihilation [29], improved understanding of bottom quark production in the standard model [30] and new Tevatron data [31] not exposing the excess all make this model already unlikely now, although there is still discussion in the literature [32] that this mass range can fully ruled out.

results for the expected cross sections, spin asymmetries and the statistical accuracy with which they could be measured at RHIC and at polarized versions of Tevatron and LHC. To gain more detailed insight into the spin asymmetries, we discuss their dependence on the transverse momentum and the rapidity of the squarks and gluinos in Section 4. Finally, some conclusions and an outlook are presented in Section 5.

2 Polarized cross sections

The leading order (LO) processes involved in squark and gluino production in a proton-proton (LHC, RHIC) or a proton-antiproton collider (Tevatron) are

- for squark-antisquark pair production

$$\begin{aligned} q + \bar{q} &\rightarrow \tilde{q} + \bar{\tilde{q}} \\ g + g &\rightarrow \tilde{q} + \bar{\tilde{q}}, \end{aligned}$$

- for squark-squark (antisquark-antisquark) production

$$\begin{aligned} q + q &\rightarrow \tilde{q} + \tilde{q} \\ \bar{q} + \bar{q} &\rightarrow \bar{\tilde{q}} + \bar{\tilde{q}}, \end{aligned}$$

- for gluino-gluino production

$$\begin{aligned} g + g &\rightarrow \tilde{g} + \tilde{g} \\ q + \bar{q} &\rightarrow \tilde{g} + \tilde{g}, \end{aligned}$$

- for squark-gluino (antisquark-gluino) production

$$\begin{aligned} q + g &\rightarrow \tilde{q} + \tilde{g} \\ \bar{q} + g &\rightarrow \bar{\tilde{q}} + \tilde{g}. \end{aligned}$$

The charge conjugated processes (in parentheses) will not be written out explicitly, they are included in the numerical results where appropriate. The matrix elements are calculated using the Feynman rules of SUSY QCD listed in [33]. The fermion number violating interactions induced by the gluinos are treated according to ref. [34].

Incoming quarks (including incoming b quarks) are assumed to be massless, such that we have $n_f = 5$ light flavours. We only consider final state squarks corresponding to the light quark flavours. All squark masses are taken equal to $m_{\tilde{q}}^2$. We do not consider in detail top squark production where these assumptions do not hold and which require a more dedicated treatment [35].

To describe the process kinematics, we assign momenta k_1 and k_2 to the incoming partons and p_1 and p_2 to the outgoing squarks and gluinos. We introduce the Mandelstam variables

$$\begin{aligned} s &= (k_1 + k_2)^2 = +2k_1 \cdot k_2 \\ t &= (k_2 - p_2)^2 = -2k_2 \cdot p_2 + p_2^2 \\ u &= (k_1 - p_2)^2 = -2k_1 \cdot p_2 + p_2^2, \end{aligned}$$

which satisfy $s + t + u = p_1^2 + p_2^2$. The following variables are also useful [26]:

$$\begin{aligned} t_1 &= (k_2 - p_2)^2 - m_{\tilde{q}}^2, & t_g &= (k_2 - p_2)^2 - m_{\tilde{g}}^2, \\ u_1 &= (k_1 - p_2)^2 - m_{\tilde{q}}^2, & u_g &= (k_1 - p_2)^2 - m_{\tilde{g}}^2. \end{aligned}$$

The colour factors corresponding to different production processes are $C_F = (N^2 - 1)/2N$, $C_O = N(N^2 - 1)$ and $C_K = (N^2 - 1)/N$, with $N = 3$.

² L -squarks and R -squarks are therefore mass-degenerate and experimentally indistinguishable.

To extract the dependence on the helicities λ , we introduce helicity projections for spinors and gluons. For the spinors we take the usual form

$$\frac{1}{2}(1 + \lambda\gamma_5) , \quad (1)$$

but more care is needed for the incoming gluons. We use an axial gauge to ensure that only physical polarization states contribute to the cross section. In this gauge, the product of the polarization vector of an incoming parton with momentum k and its complex conjugate can be written as

$$\epsilon_\mu^\pm(k, q) \cdot (\epsilon_\nu^\pm(k, q))^* = \epsilon_\mu^\pm(k, q) \cdot \epsilon_\nu^\mp(k, q) = \frac{1}{2k \cdot q} \text{Tr} \left(\frac{1 \mp \gamma^5}{2} \gamma_\mu \not{k} \gamma_\nu \not{q} \right) , \quad (2)$$

where the 'gauge vector' q is chosen conveniently. This form is independent of the representation of γ_5 .

Corresponding to the helicities $\lambda_{1,2}$ of the incoming partons, there are four different squared matrix elements

$$|\mathcal{M}|_{\lambda_1, \lambda_2}^2 ; \quad (3)$$

where $\lambda_{1,2} = -1, 1$ correspond partons with negative and positive helicity. If the final state squark chiralities are summed over, parity invariance of SUSY QCD yields

$$|\mathcal{M}|_{1,-1}^2 = |\mathcal{M}|_{-1,1}^2 \quad \text{and} \quad |\mathcal{M}|_{-1,-1}^2 = |\mathcal{M}|_{1,1}^2 . \quad (4)$$

Therefore the full polarization dependence is given by the sum and the difference

$$|\mathcal{M}|^2 = |\mathcal{M}|_{1,1}^2 + |\mathcal{M}|_{1,-1}^2 + |\mathcal{M}|_{-1,1}^2 + |\mathcal{M}|_{-1,-1}^2 , \quad (5)$$

$$\Delta|\mathcal{M}|^2 = |\mathcal{M}|_{1,1}^2 - |\mathcal{M}|_{1,-1}^2 - |\mathcal{M}|_{-1,1}^2 + |\mathcal{M}|_{-1,-1}^2 , \quad (6)$$

which we compute at leading order for all partonic squark and gluino production processes.

2.1 Polarized squared matrix elements

The Feynman diagrams for the partonic squark-antisquark production processes in Figure 1 give the squared matrix elements

$$\begin{aligned} |\mathcal{M}|^2(q_I + \bar{q}_J \rightarrow \tilde{q} + \bar{\tilde{q}}) &= \delta_{IJ} g_s^4 \left(8n_f \frac{1}{s^2} N C_F (t_1 u_1 - s m_{\tilde{q}}^2) - 8 \frac{1}{s t_g} C_F (t_1 u_1 - s m_{\tilde{q}}^2) \right) \\ &\quad + 4 \frac{g_s^4}{t_g^2} N C_F (t_1 u_1 - s(m_{\tilde{q}}^2 - m_{\tilde{g}}^2)) , \end{aligned} \quad (7)$$

$$\begin{aligned} \Delta|\mathcal{M}|^2(q_I + \bar{q}_J \rightarrow \tilde{q} + \bar{\tilde{q}}) &= -\delta_{IJ} g_s^4 \left(8n_f \frac{1}{s^2} N C_F (t_1 u_1 - s m_{\tilde{q}}^2) - 8 \frac{1}{s t_g} C_F (t_1 u_1 - s m_{\tilde{q}}^2) \right) \\ &\quad - 4 \frac{g_s^4}{t_g^2} N C_F (t_1 u_1 - s(m_{\tilde{q}}^2 + m_{\tilde{g}}^2)) , \end{aligned} \quad (8)$$

$$|\mathcal{M}|^2(g + g \rightarrow \tilde{q} + \bar{\tilde{q}}) = 4n_f g_s^4 \left[C_O \left(1 - 2 \frac{t_1 u_1}{s^2} \right) - C_K \right] \left[1 - 2 \frac{s m_{\tilde{q}}^2}{t_1 u_1} \left(1 - \frac{s m_{\tilde{q}}^2}{t_1 u_1} \right) \right] , \quad (9)$$

$$\begin{aligned} \Delta|\mathcal{M}|^2(g + g \rightarrow \tilde{q} + \bar{\tilde{q}}) &= 4n_f g_s^4 \left[C_O \left(-1 + 2 \frac{t_1 u_1}{s^2} + 2 \frac{s m_{\tilde{q}}^2}{t_1 u_1} - 4 \frac{m_{\tilde{q}}^2}{s} \right) \right. \\ &\quad \left. + C_K \left(1 - 2 \frac{s m_{\tilde{q}}^2}{t_1 u_1} \right) \right] . \end{aligned} \quad (10)$$

The contributions to the partonic squark-squark production are shown in Figure 2. This process violates

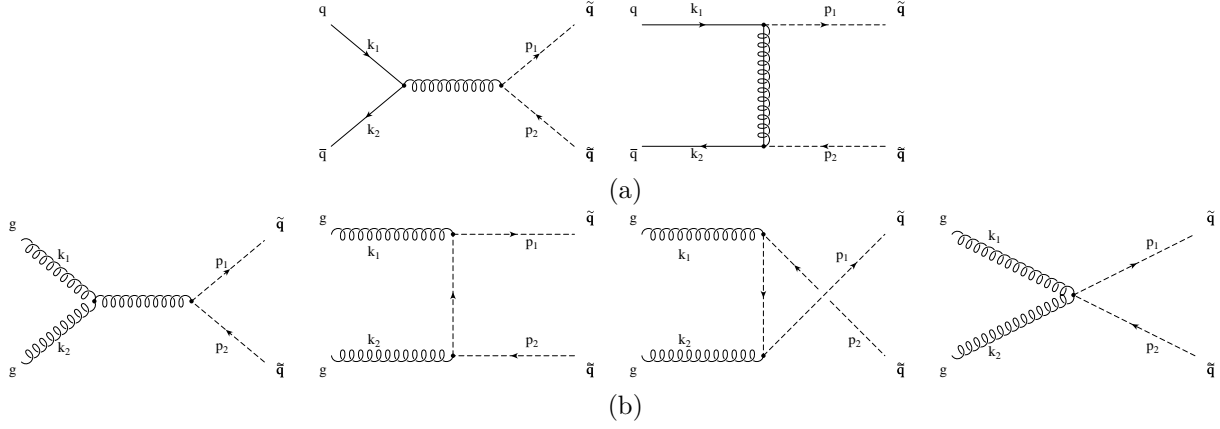


Figure 1: Feynman diagrams for squark-antisquark production: (a) quark-antiquark initial states, (b) gluon-gluon initial states.

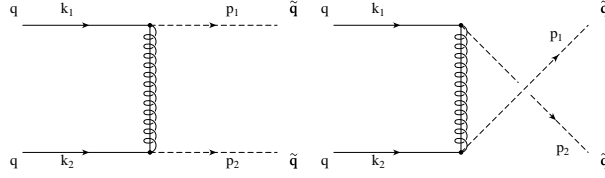


Figure 2: Feynman diagrams for squark pair production.

fermion number and occurs because of the Majorana nature of gluinos. We obtain

$$\begin{aligned}
|\mathcal{M}|^2(q + q \rightarrow \tilde{q} + \tilde{q}) &= \delta_{IJ} \left[2g_s^4 N C_F (t_1 u_1 - s m_{\tilde{q}}^2) \left(\frac{1}{t_g^2} + \frac{1}{u_g^2} \right) \right. \\
&\quad \left. + 2g_s^4 m_{\tilde{g}}^2 s \left(N C_F \left(\frac{1}{t_g^2} + \frac{1}{u_g^2} \right) - 2C_F \frac{1}{t_g u_g} \right) \right] \\
&\quad + (1 - \delta_{IJ}) \left[4g_s^4 N C_F \frac{t_1 u_1 - (m_{\tilde{q}}^2 - m_{\tilde{g}}^2) s}{t_g^2} \right] \quad (11)
\end{aligned}$$

$$\begin{aligned}
\Delta|\mathcal{M}|^2(q + q \rightarrow \tilde{q} + \tilde{q}) &= \delta_{IJ} \left[-2g_s^4 N C_F (t_1 u_1 - s m_{\tilde{q}}^2) \left(\frac{1}{t_g^2} + \frac{1}{u_g^2} \right) \right. \\
&\quad \left. + 2g_s^4 m_{\tilde{g}}^2 s \left(N C_F \left(\frac{1}{t_g^2} + \frac{1}{u_g^2} \right) - 2C_F \frac{1}{t_g u_g} \right) \right] \\
&\quad + (1 - \delta_{IJ}) \left[4g_s^4 N C_F \frac{-t_1 u_1 + (m_{\tilde{q}}^2 + m_{\tilde{g}}^2) s}{t_g^2} \right]. \quad (12)
\end{aligned}$$

The second graph only contributes for final states of same flavour. We have already taken account of the symmetry factor 1/2 for the second term corresponding to the LL or RR initial quarks of same flavour, since in these cases the final states are indistinguishable. Our results for the unpolarized matrix elements agree with previous work [26]³. The polarized matrix elements (10), (12) agree with [23], taking into account that we sum over final state squark chiralities (and symmetrize where appropriate), while [23] presents results for fixed squark chirality.

³There is a slight difference in the squared matrix elements because in ref. [26] the symmetry factors are included at the level of the cross section.

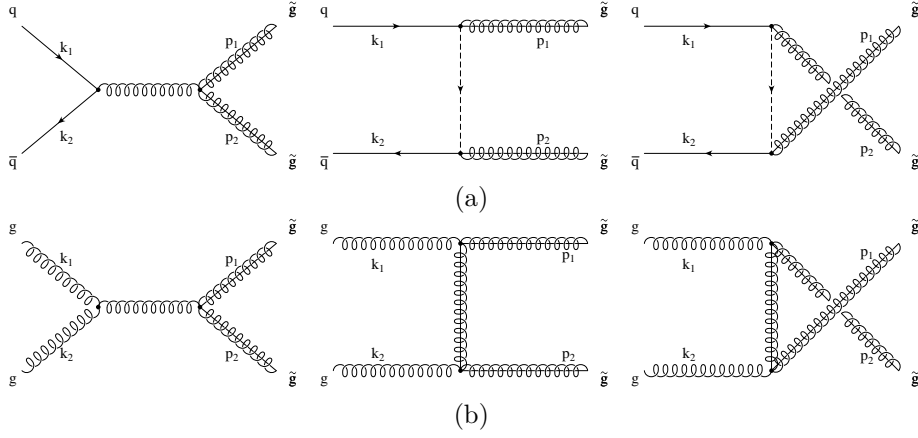


Figure 3: Feynman diagrams for gluino pair production: (a) quark-antiquark initial states, (b) gluon-gluon initial states.

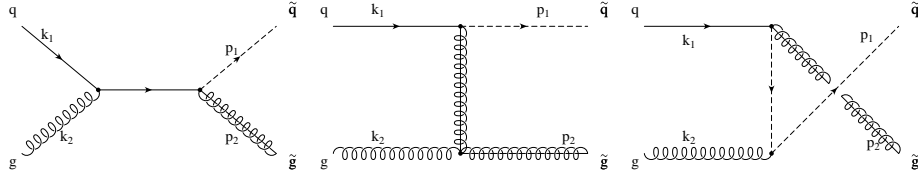


Figure 4: Feynman diagrams for squark-gluino production.

Gluino pairs can be produced in quark-antiquark or gluon-gluon annihilation as shown in Figure 3. For quark-antiquark initial states, only combinations with opposite helicities contribute and unpolarized and polarized matrix elements agree up to an overall sign. The results are:

$$\begin{aligned}
 |\mathcal{M}|^2(q + \bar{q} \rightarrow \tilde{g} + \tilde{g}) &= 2g_s^4 C_O \left[\frac{2m_{\tilde{g}}^2 s + t_g^2 + u_g^2}{s^2} + \frac{m_{\tilde{g}}^2 s + t_g^2}{st_1} + \frac{m_{\tilde{g}}^2 s + u_g^2}{su_1} \right] \\
 &\quad + g_s^4 \left[C_O \left(\frac{t_g^2}{t_1^2} + \frac{u_g^2}{u_1^2} \right) + C_K \left(2 \frac{m_{\tilde{g}}^2 s}{t_1 u_1} - \frac{t_g^2}{t_1^2} - \frac{u_g^2}{u_1^2} \right) \right], \quad (13)
 \end{aligned}$$

$$\Delta |\mathcal{M}|^2(q + \bar{q} \rightarrow \tilde{g} + \tilde{g}) = -|\mathcal{M}|^2(q + \bar{q} \rightarrow \tilde{g} + \tilde{g}), \quad (14)$$

$$|\mathcal{M}|^2(g + g \rightarrow \tilde{g} + \tilde{g}) = 4g_s^4 N C_O \left(1 - \frac{t_g u_g}{s^2} \right) \left[-2 + \frac{s^2}{t_g u_g} + 4 \frac{s m_{\tilde{g}}^2}{t_g u_g} \left(1 - \frac{s m_{\tilde{g}}^2}{t_g u_g} \right) \right], \quad (15)$$

$$\Delta |\mathcal{M}|^2(g + g \rightarrow \tilde{g} + \tilde{g}) = 4g_s^4 N C_O \left[m_{\tilde{g}}^2 \left(\frac{4}{s} - \frac{6s}{t_g u_g} + 2 \frac{s^3}{u_g^2 t_g^2} \right) + 3 - 2 \frac{t_g u_g}{s^2} - \frac{s^2}{t_g u_g} \right]. \quad (16)$$

For all gluino pair production matrix elements, we include a symmetry factor of 1/2 to account for the production of identical Majorana fermions. Our results agree with ref. [26], once the symmetry factor is taken into account. Finally, squark-gluino final states are produced through the quark-gluon scattering in

Figure 4, which yields

$$|\mathcal{M}|^2(q + g \rightarrow \tilde{q} + \tilde{g}) = 2g_s^4 \left[C_O \left(1 - 2\frac{su_1}{t_g^2} \right) - C_K \right] \times \left[-\frac{t_g}{s} + 2\frac{(m_{\tilde{g}}^2 - m_{\tilde{q}}^2)t_g}{su_1} \left(1 + \frac{m_{\tilde{q}}^2}{u_1} + \frac{m_{\tilde{g}}^2}{t_g} \right) \right], \quad (17)$$

$$\begin{aligned} \Delta|\mathcal{M}|^2(q + g \rightarrow \tilde{q} + \tilde{g}) &= 2g_s^4 \left[C_O \left[m_{\tilde{g}}^2 \left(4\frac{s}{t_g^2} + 2\frac{s}{t_g u_1} + \frac{2}{t_g} \right) \right. \right. \\ &\quad \left. \left. - \left(2 + \frac{t_g}{s} + 2\frac{u_g}{s} + 2\frac{s}{t_g} + 4\frac{u_g}{t_g} + 2\frac{u_g}{u_1} \right) \right] \right. \\ &\quad \left. + C_K \left(2\frac{m_{\tilde{g}}^2}{u_1} - 2\frac{t_g u_g}{su_1} + \frac{t_g}{s} \right) \right]. \end{aligned} \quad (18)$$

The unpolarized expressions agree with ref. [26]. The polarized matrix elements (16), (18) agree with [23], again taking into account the different treatment of symmetry factors and final state summations.

2.2 Polarized partonic cross sections

The inclusive cross section for a particular partonic reaction where the two partons i and j in the initial state have helicities λ_i, λ_j is given by ⁴

$$\hat{\sigma}_{\lambda_i, \lambda_j} = \frac{K_{ij}}{2s} \int \frac{d^3 p_1}{(2\pi)^3 2E_1} \frac{d^3 p_2}{(2\pi)^3 2E_2} (2\pi)^4 \delta(k_1 + k_2 - p_1 - p_2) |\mathcal{M}_{\lambda_i, \lambda_j}|^2. \quad (19)$$

The factor K_{ij} accounts for the average over the initial state colours. We have $K_{q\bar{q}, qq} = 1/N^2$ for quark-antiquark or quark-quark initial states, $K_{gg} = 1/(N^2 - 1)^2$ for gluon-gluon initial states and $K_{qg} = 1/N/(N^2 - 1)$ for quark-gluon initial states. The above expression can be transformed into an integral over Mandelstam invariants

$$\hat{\sigma}_{\lambda_i, \lambda_j} = K_{ij} \int du \int dt \frac{1}{16\pi s^2} \Theta((t - m^2)(u - m^2) - sm^2) \Theta(s - 4m^2) \delta(s + t + u - m_1^2 - m_2^2) |\mathcal{M}_{\lambda_i, \lambda_j}|^2 \quad (20)$$

where $m = (m_1 + m_2)/2$ is the average mass of the final state particles. For our goals we define the unpolarized and polarized cross sections by

$$\hat{\sigma} = \frac{1}{4} (\hat{\sigma}_{1,1} + \hat{\sigma}_{1,-1} + \hat{\sigma}_{-1,1} + \hat{\sigma}_{-1,-1}), \quad (21)$$

$$\Delta\hat{\sigma} = \frac{1}{4} (\hat{\sigma}_{1,1} - \hat{\sigma}_{1,-1} - \hat{\sigma}_{-1,1} + \hat{\sigma}_{-1,-1}), \quad (22)$$

where the symmetry factor 1/4 accounts for an average over the partonic polarizations in the initial state.

⁴We have omitted the labels i, j for the cross section where they are obvious.

Carrying out the integration we obtain the following integrated cross sections which agree with [26]:

$$\begin{aligned}
\hat{\sigma}(q_I + \bar{q}_J \rightarrow \tilde{q} + \bar{\tilde{q}}) &= \delta_{IJ} \frac{C_F n_f \pi \alpha_s^2}{N s} \beta_{\tilde{q}} \left[\frac{1}{3} - \frac{4m_{\tilde{q}}^2}{3s} \right] \\
&+ \delta_{IJ} \frac{C_F \pi \alpha_s^2}{N^2 s} \left[\beta_{\tilde{q}} \left(1 + \frac{2m_-^2}{s} \right) + \left(\frac{2m_{\tilde{g}}^2}{s} + \frac{2m_-^4}{s^2} \right) L_1 \right] \\
&+ \frac{C_F \pi \alpha_s^2}{N s} \left[\beta_{\tilde{q}} \left(-1 - \frac{m_-^4}{m_{\tilde{g}}^2 s + m_-^4} \right) + \left(-1 - \frac{2m_-^2}{s} \right) L_1 \right], \tag{23}
\end{aligned}$$

$$\begin{aligned}
\hat{\sigma}(g + g \rightarrow \tilde{q} + \bar{\tilde{q}}) &= \frac{n_f \pi \alpha_s^2}{3(N^2 - 1)^2 s^3} [C_O (\beta_{\tilde{q}} (2s^2 + 22sm_{\tilde{q}}^2) + 12L_{\tilde{q}} sm_{\tilde{q}}^2) \\
&- C_K (\beta_{\tilde{q}} (3s^2 + 12sm_{\tilde{q}}^2) + 12L_{\tilde{q}} sm_{\tilde{q}}^2 - 24L_{\tilde{q}} m_{\tilde{q}}^4)], \tag{24}
\end{aligned}$$

$$\begin{aligned}
\hat{\sigma}(q_I + q_J \rightarrow \tilde{q} + \tilde{q}) &= \frac{C_F \pi \alpha_s^2}{N s} \left[\beta_{\tilde{q}} \left(-1 - \frac{m_-^4}{m_{\tilde{g}}^2 s + m_-^4} \right) + \left(-1 - \frac{2m_-^2}{s} \right) L_1 \right] \\
&+ \delta_{IJ} \frac{C_F \pi \alpha_s^2}{N^2 s} \left[\frac{2m_{\tilde{g}}^2}{s + 2m_-^2} L_1 \right], \tag{25}
\end{aligned}$$

$$\begin{aligned}
\hat{\sigma}(q + \bar{q} \rightarrow \tilde{g} + \tilde{g}) &= \frac{C_O \pi \alpha_s^2}{N^2 s} \beta_{\tilde{g}} \left(\frac{1}{3} + \frac{2m_{\tilde{g}}^2}{3s} \right) \\
&+ \frac{C_O \pi \alpha_s^2}{N^2 s} \left[\beta_{\tilde{g}} \left(-\frac{1}{2} - \frac{m_-^2}{s} \right) + \left(\frac{m_{\tilde{g}}^2}{s} + \frac{m_-^4}{s^2} \right) L_2 \right] \\
&+ \frac{\pi \alpha_s^2}{s} \left[\frac{C_O - C_K}{N^2} \left(\beta_{\tilde{g}} \left(\frac{1}{2} + \frac{m_-^4}{2(m_{\tilde{g}}^2 s + m_-^4)} \right) - L_2 \frac{m_-^2}{s} \right) \right. \\
&\quad \left. - \frac{C_K}{N^2} \left(\frac{m_{\tilde{g}}^2}{s - 2m_-^2} \right) L_2 \right], \tag{26}
\end{aligned}$$

$$\hat{\sigma}(g + g \rightarrow \tilde{g} + \tilde{g}) = \frac{8NC_O \pi \alpha_s^2}{9(N^2 - 1)^2 s} \left[\beta_{\tilde{g}} \left(-3 - \frac{51m_{\tilde{g}}^2}{4s} \right) + \left(-\frac{9}{4} - \frac{9m_{\tilde{g}}^2}{s} + \frac{9m_{\tilde{g}}^4}{s^2} \right) L_{\tilde{g}} \right], \tag{27}$$

$$\begin{aligned}
\hat{\sigma}(q + g \rightarrow \tilde{q} + \tilde{g}) &= -\frac{\pi \alpha_s^2}{4N(N^2 - 1)s^3} [C_K (4L_3(m_-^4 - sm_-^2) + \kappa(s - 7m_-^2)) \\
&+ C_O (-4L_3(m_-^4 - sm_-^2 + 2m_{\tilde{q}}^2 m_-^2) \\
&+ 4L_4(2sm_-^2 - 2m_{\tilde{q}}^2 m_-^2 + s^2) + \kappa(3s + 15m_-^2))], \tag{28}
\end{aligned}$$

with the following functions and constants:

$$\begin{aligned}
\alpha_s &= g_s^2/4\pi \\
\beta_{\tilde{q}} &= \sqrt{1 - \frac{4m_{\tilde{q}}^2}{s}} & \beta_{\tilde{g}} &= \sqrt{1 - \frac{4m_{\tilde{g}}^2}{s}} \\
m_-^2 &= m_{\tilde{g}}^2 - m_{\tilde{q}}^2 & \kappa &= \sqrt{(s - m_{\tilde{g}}^2 - m_{\tilde{q}}^2)^2 - 4m_{\tilde{g}}^2 m_{\tilde{q}}^2} \\
L_1 &= \log \left(\frac{s + 2m_-^2 - s\beta_{\tilde{q}}}{s + 2m_-^2 + s\beta_{\tilde{q}}} \right) & L_2 &= \log \left(\frac{s - 2m_-^2 - s\beta_{\tilde{g}}}{s - 2m_-^2 + s\beta_{\tilde{g}}} \right) \\
L_3 &= \log \left(\frac{s - m_-^2 - \kappa}{s - m_-^2 + \kappa} \right) & L_4 &= \log \left(\frac{s + m_-^2 - \kappa}{s + m_-^2 + \kappa} \right) \\
L_{\tilde{q}} &= \log \left(\frac{1 - \beta_{\tilde{q}}}{1 + \beta_{\tilde{q}}} \right) & L_{\tilde{g}} &= \log \left(\frac{1 - \beta_{\tilde{g}}}{1 + \beta_{\tilde{g}}} \right). \tag{29}
\end{aligned}$$

The new result concerns the polarized cross sections $\Delta\hat{\sigma}$ which read:

$$\begin{aligned}\Delta\hat{\sigma}(q_I + \bar{q}_J \rightarrow \tilde{q} + \bar{\tilde{q}}) &= -\delta_{IJ} \frac{C_F n_f \pi \alpha_s^2}{N s} \beta_{\tilde{q}} \left[\frac{1}{3} - \frac{4m_{\tilde{q}}^2}{3s} \right] \\ &\quad - \delta_{IJ} \frac{C_F \pi \alpha_s^2}{N^2 s} \left[\beta_{\tilde{q}} \left(1 + \frac{2m_-^2}{s} \right) + \left(\frac{2m_{\tilde{g}}^2}{s} + \frac{2m_-^4}{s^2} \right) L_1 \right] \\ &\quad - \frac{C_F \pi \alpha_s^2}{N s} \left[\beta_{\tilde{q}} \left(-3 - \frac{m_-^4}{m_{\tilde{g}}^2 s + m_-^4} \right) + \left(-1 - \frac{2m_-^2}{s} \right) L_1 \right],\end{aligned}\quad (30)$$

$$\begin{aligned}\Delta\hat{\sigma}(g + g \rightarrow \tilde{q} + \bar{\tilde{q}}) &= -\frac{n_f \pi \alpha_s^2}{3(N^2 - 1)^2 s^3} [C_O (\beta_{\tilde{q}}(2s^2 + 10sm_{\tilde{q}}^2) + 12L_{\tilde{q}} sm_{\tilde{q}}^2) \\ &\quad + C_K (-3\beta_{\tilde{q}} s^2 - 12sm_{\tilde{q}}^2 L_{\tilde{q}})],\end{aligned}\quad (31)$$

$$\begin{aligned}\Delta\hat{\sigma}(q_I + q_J \rightarrow \tilde{q} + \bar{\tilde{q}}) &= \frac{C_F \pi \alpha_s^2}{N s} \left[\beta_{\tilde{q}} \left(3 - \frac{m_-^4}{m_{\tilde{g}}^2 s + m_-^4} \right) + \left(1 + \frac{2m_-^2}{s} \right) L_1 \right] \\ &\quad + \delta_{IJ} \frac{C_F \pi \alpha_s^2}{N^2 s} \left[\frac{2m_{\tilde{g}}^2}{s + 2m_-^2} L_1 \right],\end{aligned}\quad (32)$$

$$\Delta\hat{\sigma}(q + \bar{q} \rightarrow \tilde{g} + \bar{\tilde{g}}) = -\hat{\sigma}(q\bar{q} \rightarrow \tilde{g}\bar{\tilde{g}}),\quad (33)$$

$$\Delta\hat{\sigma}(g + g \rightarrow \tilde{g} + \bar{\tilde{g}}) = \frac{NC_O}{(N^2 - 1)^2} \frac{\pi \alpha_s^2}{s} \left[\beta_{\tilde{g}} \left(\frac{20}{3} + \frac{10m_{\tilde{g}}^2}{3s} \right) + \left(2 + \frac{4m_{\tilde{g}}^2}{s} \right) L_{\tilde{g}} \right],\quad (34)$$

$$\begin{aligned}\Delta\hat{\sigma}(q + g \rightarrow \tilde{q} + \bar{\tilde{q}}) &= \frac{\pi \alpha_s^2}{4N(N^2 - 1)s^3} [C_K (4L_3 sm_{\tilde{q}}^2 + \kappa(s - 3m_-^2)) \\ &\quad + C_O (-4L_3 sm_{\tilde{q}}^2 + 4L_4 s(s + 2m_-^2) + \kappa(11s + 3m_-^2))].\end{aligned}\quad (35)$$

In all cross sections, the production threshold factor $\Theta(s - 4m^2)$ is implicit.

2.3 Polarized hadronic cross sections

The measured hadronic cross sections $\sigma(A + B \rightarrow X)$ are obtained by weighting the partonic cross sections $\hat{\sigma}_{\lambda_1, \lambda_2}$ with the probability of finding the initial partons with the corresponding helicity orientations inside the initial hadrons A and B which are assumed to be polarized. We are particularly interested in the polarized cross section $\Delta\hat{\sigma}$. It is useful to define the unpolarized and polarized cross sections by

$$\begin{aligned}\sigma(A + B \rightarrow X) &= \sum_{\substack{\text{process} \\ i+j \rightarrow X}} \int_0^1 dx_1 dx_2 \left(p_{i/A}(x_1) p_{j/B}(x_2) \right. \\ &\quad \left. + p_{j/A}(x_1) p_{i/B}(x_2) \right) \hat{\sigma}_{i+j \rightarrow X}(s),\end{aligned}\quad (36)$$

$$\begin{aligned}\Delta\sigma(A + B \rightarrow X) &= \sum_{\substack{\text{process} \\ i+j \rightarrow X}} \int_0^1 dx_1 dx_2 \left(\Delta p_{i/A}(x_1) \Delta p_{j/B}(x_2) \right. \\ &\quad \left. + \Delta p_{j/A}(x_1) \Delta p_{i/B}(x_2) \right) \Delta\hat{\sigma}_{i+j \rightarrow X}(s),\end{aligned}\quad (37)$$

S is the centre-of-mass energy squared at the hadronic and $s = Sx_1x_2$ at the partonic level. $p_{k/H}(x)$ and $\Delta p_{k/H}(x)$ are the unpolarized and polarized parton distribution functions. The unpolarized distributions parametrise the probability of finding a parton k inside a hadron H with momentum fraction x and any helicity, whereas the the polarized distributions give the difference between the probabilities of finding a parton with its spin parallel and anti-parallel to that of the hadron. The summation includes all quark and antiquark flavours and the gluon.

The above hadronic cross sections can be measured experimentally by studying production cross sections with different but fixed longitudinal spin-orientations for the incoming hadrons $\sigma^{\pm\pm}$, where each (\pm) denotes the longitudinal spin orientation (in direction of motion or opposite) of one of the incoming hadrons:

$$\sigma = \frac{1}{4} (\sigma^{++} + \sigma^{+-} + \sigma^{-+} + \sigma^{--}) , \quad (38)$$

$$\Delta\sigma = \frac{1}{4} (\sigma^{++} - \sigma^{+-} - \sigma^{-+} + \sigma^{--}) . \quad (39)$$

From these, one can construct the production asymmetry

$$A = \frac{\Delta\sigma}{\sigma} . \quad (40)$$

Because several uncertainties in the normalisation cancel, A can be measured with less systematic errors than the individual cross sections.

3 Inclusive hadronic asymmetries

To illustrate the potential of polarized hadron colliders, we consider the following three possibilities:

RHIC: At present, the only polarized hadron collider is the relativistic heavy ion collider (RHIC) at BNL, which collides two longitudinally polarized proton beams at centre-of-mass energies $\sqrt{S} = 200$ to 500 GeV. We consider only $\sqrt{S} = 500$ GeV, with a beam polarization of 70% for both beams and an integrated luminosity of 800 pb⁻¹, according to the design parameters [6].

Tevatron: The Fermilab Tevatron is an unpolarized proton-antiproton collider, which is currently operating at $\sqrt{S} = 1.96$ TeV. In the current run, an integrated luminosity of 10 fb⁻¹ is anticipated. We take these values and a hypothetical 70% polarization for both beams.

LHC: At present under construction at CERN, the large hadron collider will soon provide proton-proton collisions at $\sqrt{S} = 14$ TeV. To examine the physics prospects of a hypothetical polarized physics programme, we assume an integrated luminosity of 500 fb⁻¹ and beam polarizations of 70 %.

We numerically integrated the formulae for the total cross section (36) and for the hadronic polarisation difference (37) to calculate the asymmetry $A(Z)$ (formula (40)) for all squark and gluino final states $X = \tilde{g}\tilde{g}, \tilde{g}\tilde{q}/\tilde{g}\tilde{\bar{q}}, \tilde{q}\tilde{q}/\tilde{q}\tilde{\bar{q}}, \tilde{q}\tilde{\bar{q}}$. The GRV98 unpolarized parton density parametrisation [36] for the u, d, s quarks was used. These distributions are determined in a fixed flavour number scheme [37], and thus do not contain c and b quarks. As in the unpolarized calculation of [26], we take these from the the older GRV92 parametrisation [38]. For the polarised parton distributions, we used the GRSV2000 parametrisation [9] with its "standard" scenario, which contains only u, d, s quarks. The polarized heavy quark distributions are expected to be negligible compared to unpolarized ones. We use throughout the leading order densities as well as the leading order strong coupling constant with $\lambda_{QCD}^{n_f=5} = 132$ MeV ($\alpha_s^{LO}(M_Z) = 0.125$).

3.1 Scale dependence

Both the QCD coupling constant α_s and the parton distribution functions depend on the scale at which they are probed. Working at leading order the production cross sections are therefore scale-dependent. Since polarized and unpolarized cross sections scale with the same power of α_s , the renormalisation scale dependence drops out in the asymmetry. The remaining dependence on the factorisation scale of the parton distribution functions is weak because the evolution of the distribution functions in the numerator and denominator are comparable. This is illustrated in Figure 3 for the three colliders: the scale dependence of the asymmetry almost disappears. This could be taken as an indication that the leading order spin asymmetry does not receive substantial corrections in higher order and is sufficient for our exploratory studies. We will set the renormalisation and factorisation scale to the average final state mass m .

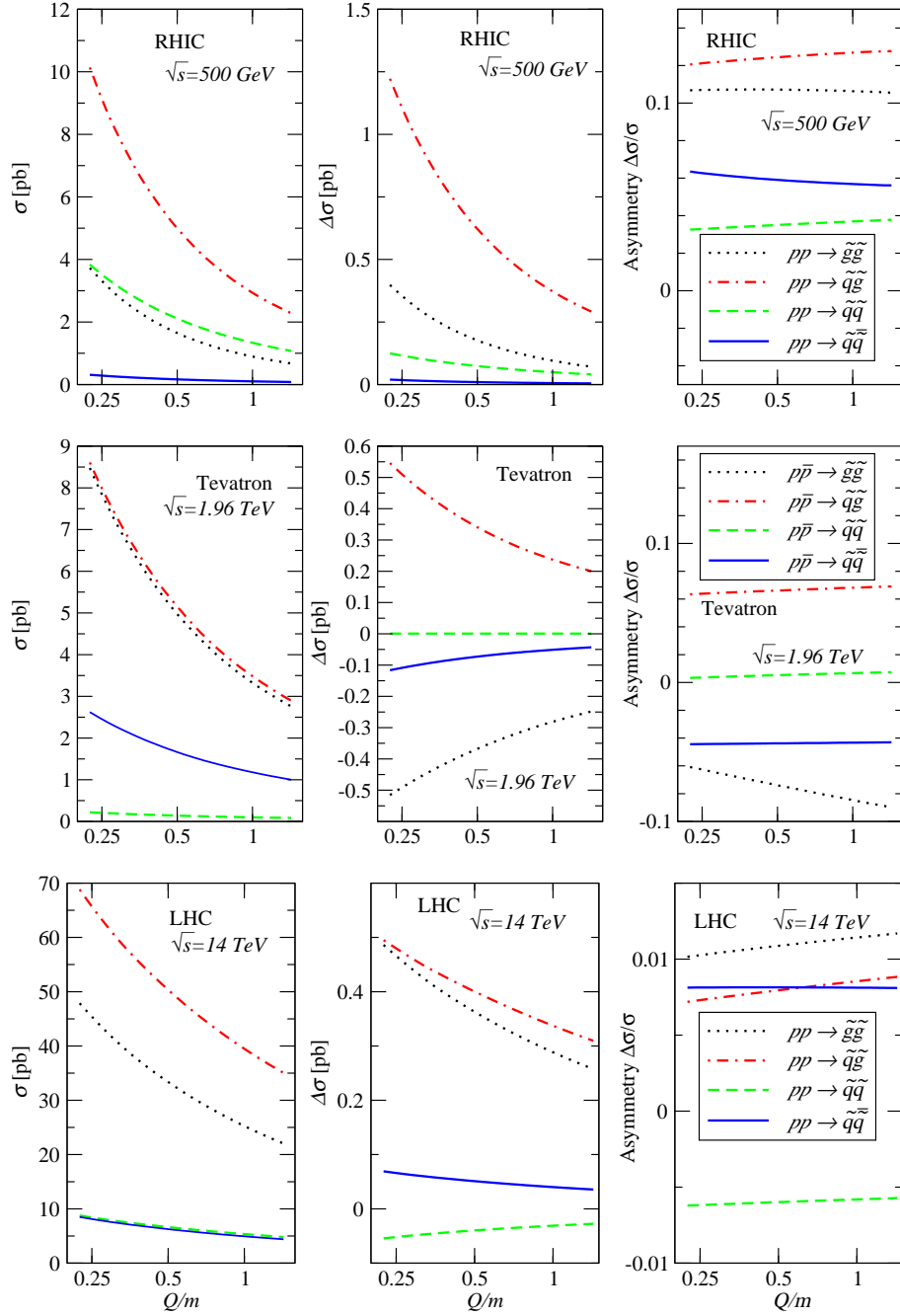


Figure 5: Dependence of total unpolarized and polarized production cross sections and asymmetry on the renormalisation and mass factorisation scale Q for RHIC, Tevatron and LHC. The mass parameters are for RHIC: $m_{\tilde{q}} = 100$ GeV, $m_{\tilde{g}} = 80$ GeV; Tevatron: $m_{\tilde{q}} = 280$ GeV, $m_{\tilde{g}} = 200$ GeV and LHC: $m_{\tilde{q}} = 600$ GeV, $m_{\tilde{g}} = 500$ GeV. Q is the renormalisation and factorisation scale for the parton distributions and $m = (m_1 + m_2)/2$, where m_1 and m_2 are the mass of the produced particles.

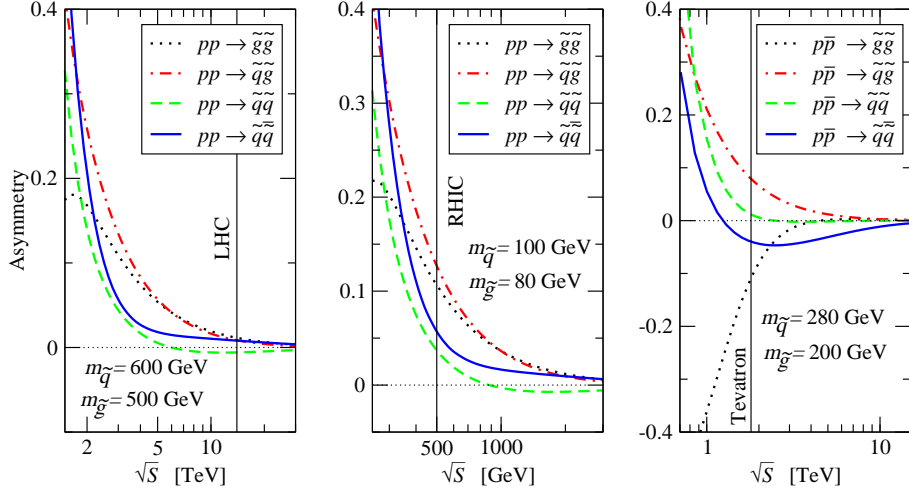


Figure 6: Asymmetry as a function of the hadronic centre of mass energy.

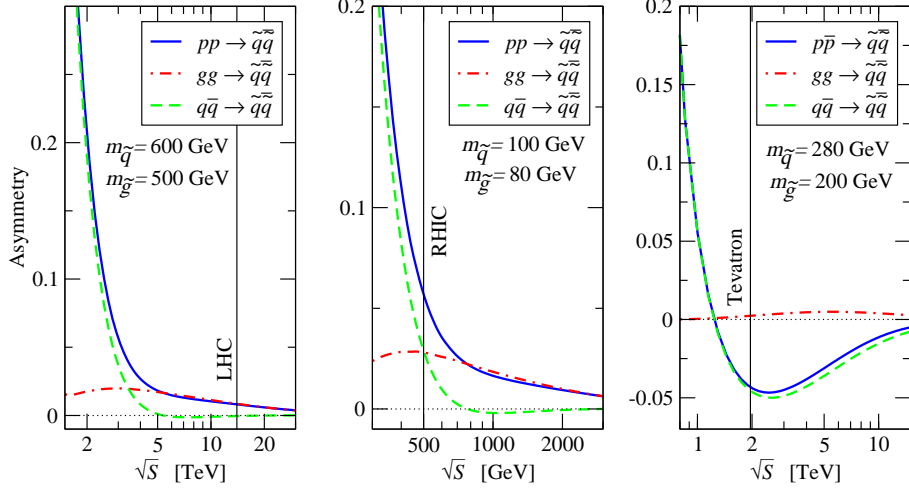


Figure 7: Quark-antiquark and gluon pair contributions to asymmetry of the squark-antisquark production as a function of the hadronic centre of mass energy.

3.2 Asymmetries at different colliders

Figure 6 shows the asymmetries for different colliders and centre-of-mass energies for fixed squark and gluino masses. For the masses chosen, the asymmetries at LHC and RHIC are quite similar; only the signs in squark-squark production are different as a consequence of the rapid falloff of the polarisation difference with S . In contrast, the asymmetries at proton-antiproton colliders are quite different; both the gluino-gluino and the squark-antisquark asymmetries are negative.

These two processes obtain contributions from the quark-antiquark initial state and from the gluon pair initial state. The relative contributions to the asymmetry from the quark-antiquark and gluon pair initial states are illustrated in more detail Figures 7 and 8. For squark-antisquark production, Figure 7, we find that for pp machines (LHC and RHIC), the quark-antiquark initial state is more important for \sqrt{S} below four times the squark mass, whereas at higher \sqrt{S} gluon pairs dominate. In $p\bar{p}$ collisions, on the other hand, the quark-antiquark initial state dominates always (except where its contribution changes sign – at $\sqrt{S} \simeq 1,2$ TeV in our case). For the gluino pair production, Figure 8, the gluon initial state (positive

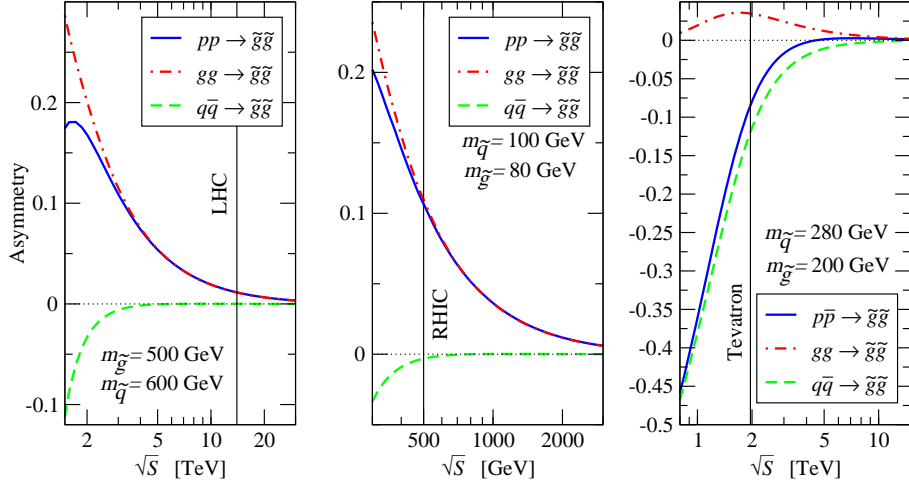


Figure 8: Quark-antiquark and gluon pair contributions to the asymmetry for the gluino pair production as a function of the hadronic centre of mass energy.

contribution) dominates in pp collisions (LHC and RHIC), and the quark-antiquark initial state (negative contribution) in $p\bar{p}$ collisions. At LHC, the latter contribution turns positive because the polarised density product $\Delta q(x)\Delta\bar{q}(x)$ changes sign in the neighbourhood of $x = 0.2$, which is only accessible at the LHC with our choice of mass parameters.

The asymmetries are largest in the neighbourhood of the production threshold, $\sqrt{S}/2 \simeq m$ where particle production requires x to be near 1. Since the parton distributions are steeply falling and badly known for $x \rightarrow 1$, these apparently large asymmetries correspond to vanishing cross sections and cannot be reliably predicted.

Figures 7 and 8 also illustrate the uncertainty in the predicted asymmetry due to the uncertainties in the (polarized) parton distribution functions. Most sparticle production processes (except squark–squark production) at LHC are dominated by gluon initial states. Since the polarized gluon distribution is not well constrained by experimental data at present, one should consider the predictions for the production asymmetries at LHC as uncertain. The present fits of polarized parton distributions come largely from polarized deep inelastic scattering data which probe only the polarized quark distributions. The polarized gluon distributions are obtained from the evolution of the polarized structure functions, and are therefore only weakly constrained. Thus the predicted asymmetries are less reliable in energy and mass ranges where initial gluons are important. However, data on single inclusive hadron production and on jet production from RHIC will soon improve our knowledge on the polarized gluon distribution, such that more accurate predictions will become feasible. On the other hand, squark-squark production asymmetries which only requires quark-quark initial states are already quite accurate.

3.3 Sparticle Mass Dependence

The squark and gluino production cross sections and asymmetries depend on their masses. In the absence of observational evidence for supersymmetric particle production, these masses are unknown. Within the MSSM, one can derive the mass bounds [27] $m_{\tilde{q}} > 250$ GeV, $m_{\tilde{g}} > 195$ GeV; in more complicated scenarios they are significantly weaker. To exhibit the spin asymmetries one could expect, we scan the space of squark and gluino mass parameters. The results are displayed in Figures 9–12.

While the unpolarized and polarized cross sections fall rapidly with increasing sparticle masses, the asymmetry (ratio of polarized to unpolarized cross section) rises. This is because the ratio of polarized to unpolarized parton distributions is largest for $x \simeq 1$. In all squark-antisquark and squark-squark production asymmetries, one observes a sensitivity to the gluino mass, although the gluino appears in these processes only as an exchange particle. This feature could eventually be used to put constraints on the gluino mass

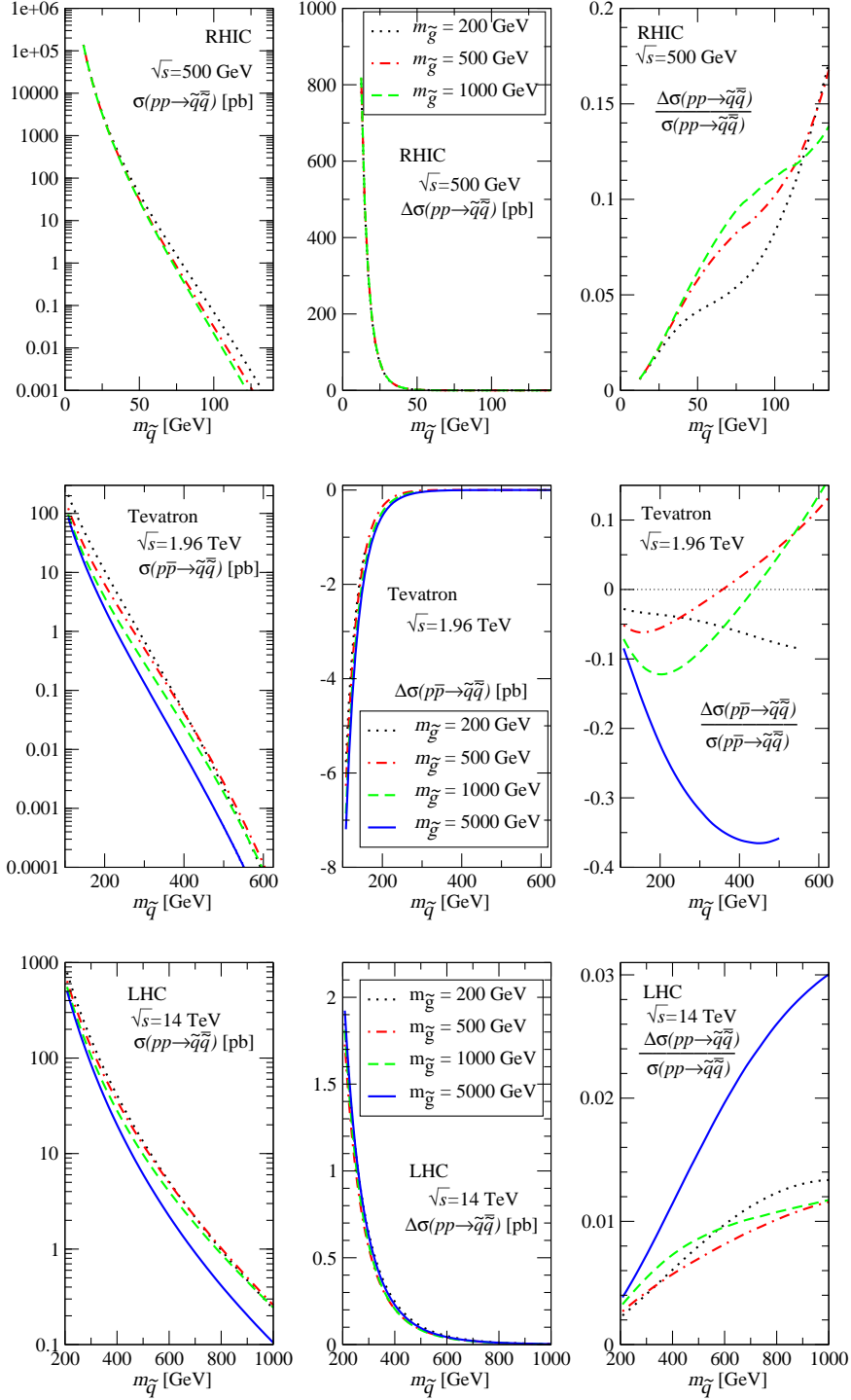


Figure 9: Total cross section, polarisation difference and asymmetry for the production of squark-antisquark for the three colliders LHC, Tevatron and RHIC.

from asymmetries in squark production, even if direct observation of the gluino is beyond the reach of the available collider. A similar determination from the unpolarized cross section would require a very precise

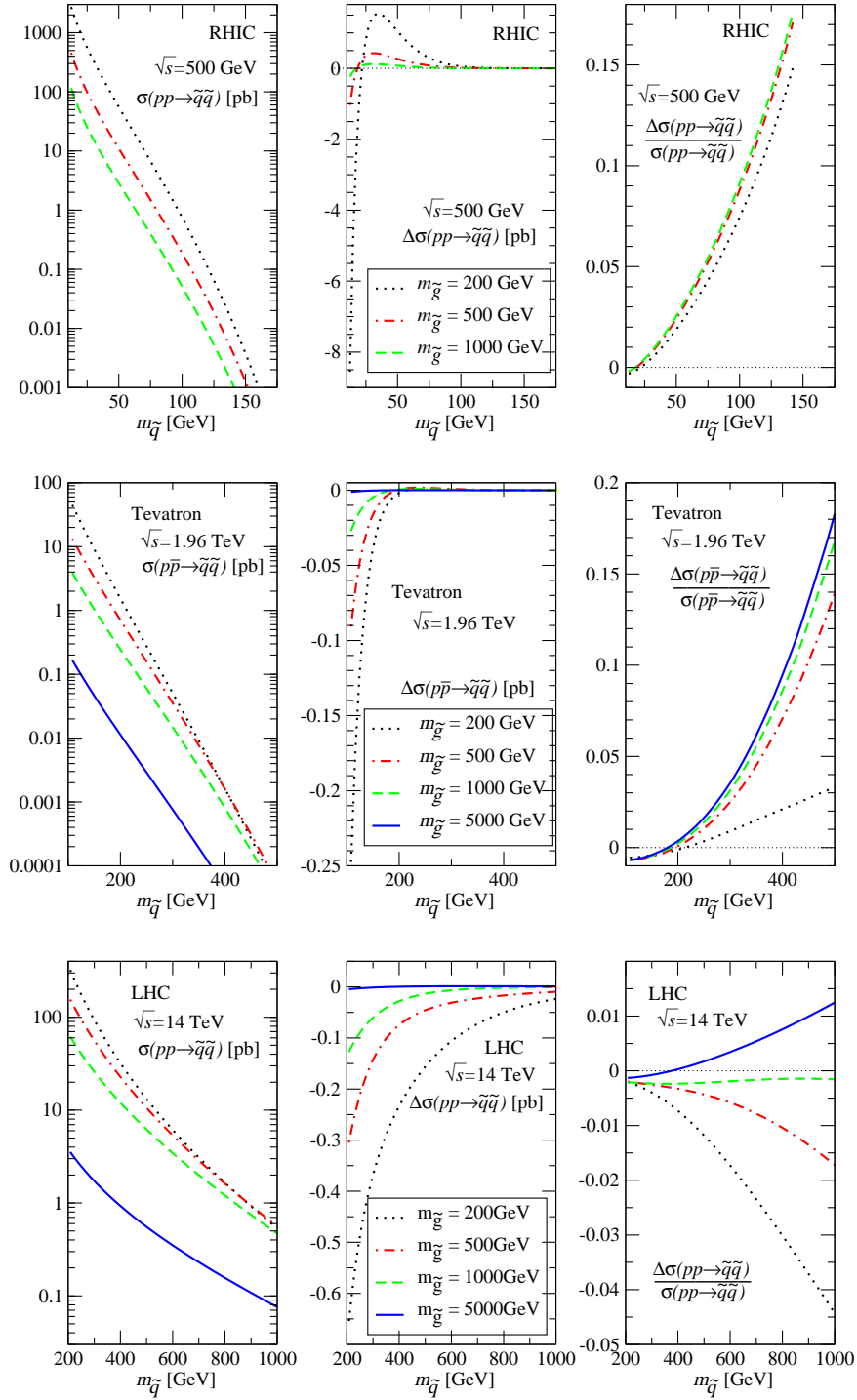


Figure 10: Total cross section, polarisation difference and asymmetry for the production of squark-squark and anti-squark-anti-squark for the three colliders LHC, Tevatron and RHIC.

absolute measurement of this cross section, and an equally precise theoretical understanding. In contrast, gluino production is only weakly dependent on the squark mass.

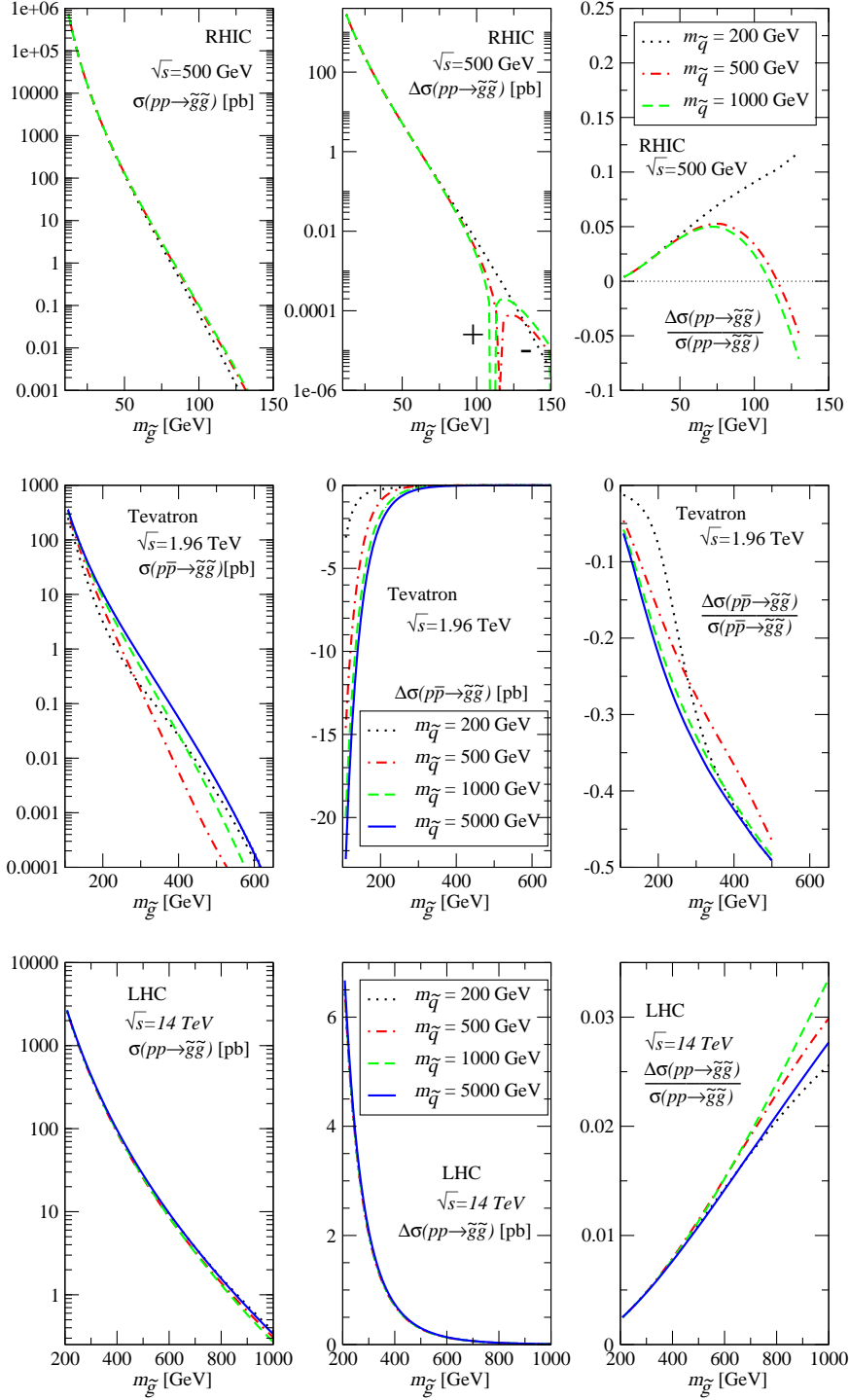


Figure 11: Total cross section, polarisation difference and asymmetry for the production of gluino-gluino for the three colliders LHC, Tevatron and RHC.

We see that production asymmetries can reach 10%–20% for sparticle production at RHC and Tevatron and up to 4% at the LHC for the ranges of parameters plotted here. The reason for this lies again in

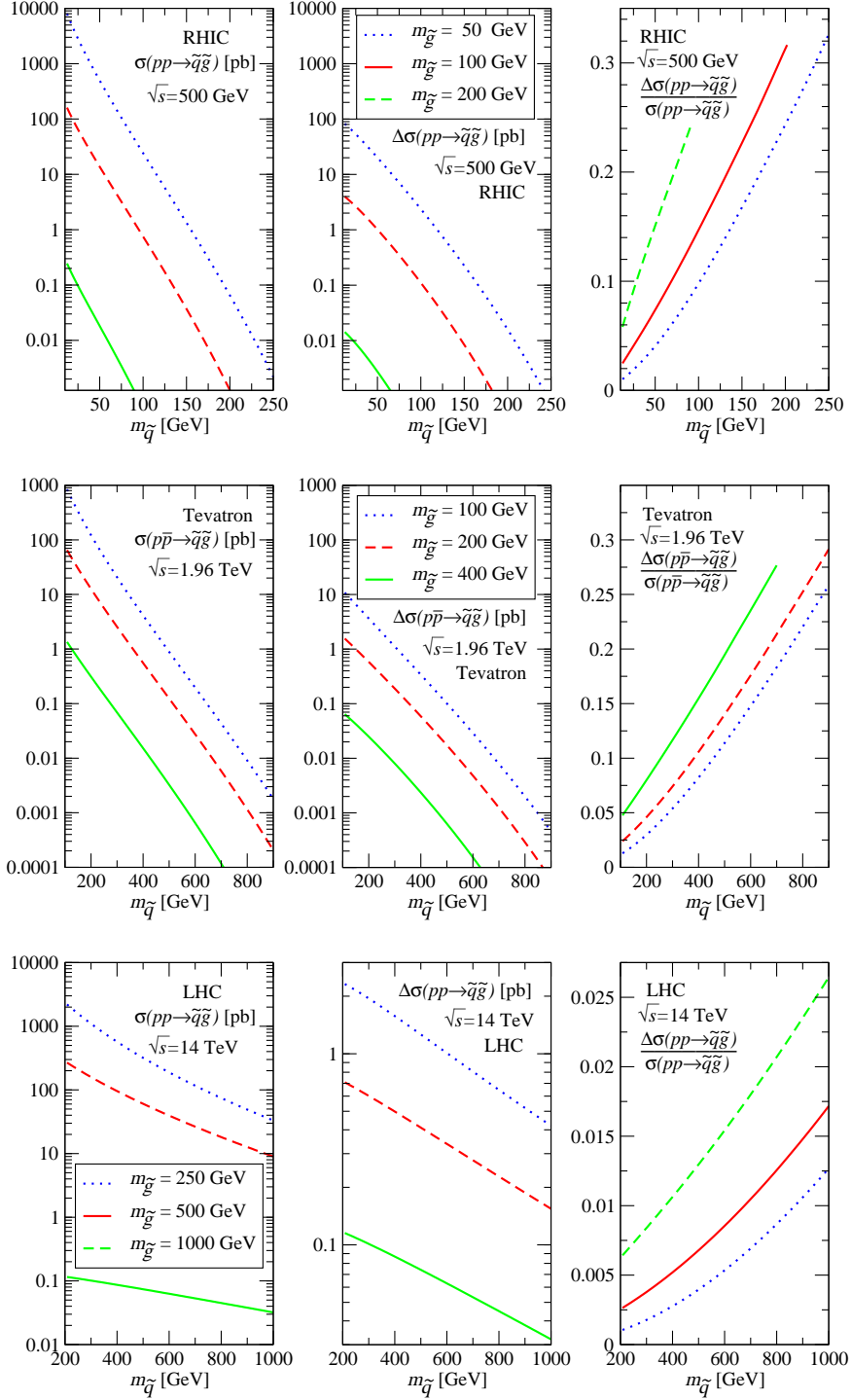


Figure 12: Total cross section, polarisation difference and asymmetry for the production of squark(antisquark)-gluino for the three colliders LHC, Tevatron and RHC.

the mass dependence of the asymmetry; For higher particle masses, asymmetries at LHC are even larger. However, as will be shown in Section 3.4 below, not enough events can be observed at these masses to allow

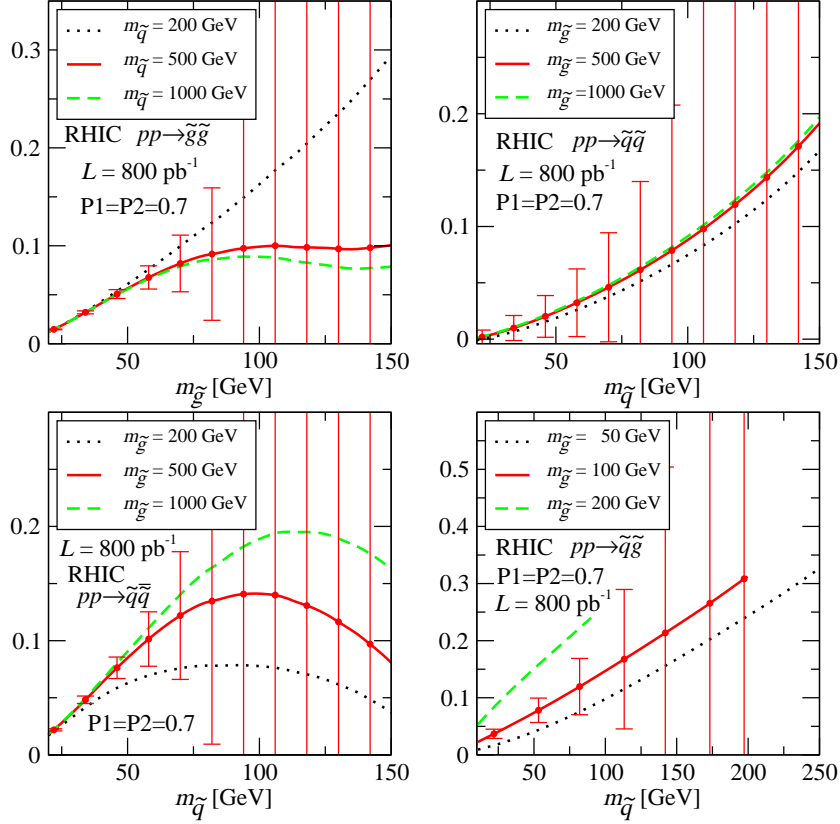


Figure 13: Statistical error on the asymmetry for the RHIC. We have assumed a polarisation of 70% and a total integrated luminosity of 800 pb^{-1} .

a measurement of an asymmetry.

3.4 Statistical Errors

From the unpolarized cross sections we can estimate the statistical errors for the measurement of the spin asymmetries. We will use the luminosity specifications postulated above for RHIC and the polarized options of Tevatron and LHC.

According to [6], the experimentally measured asymmetry is given by:

$$A = \frac{1}{P_1 P_2} \frac{N_+ - N_-}{N_+ + N_-}, \quad (41)$$

where P_1 and P_2 are the polarisation of the two colliding beams and N_{\pm} are defined as follows

$$N_+ = N_{++} + N_{--} \quad , \quad N_- = N_{+-} + N_{-+}.$$

N_{rs} is the number of events counted with beams s - and r -polarised, normalised by the luminosity for this polarisation configuration. The statistical error ΔA for this measurement is given by:

$$\Delta A^2 = \langle (A - \langle A \rangle)^2 \rangle = \langle \delta A^2 \rangle. \quad (42)$$

We assume that the results of the counts for N_+ and N_- are Poisson distributed and that the error on N_{\pm} due to the errors on the polarisation of the beams and on the luminosity are small compared to the deviation due to the Poisson statistic. The error on N_{\pm} is then

$$\Delta N_{\pm}^2 = N_{\pm},$$

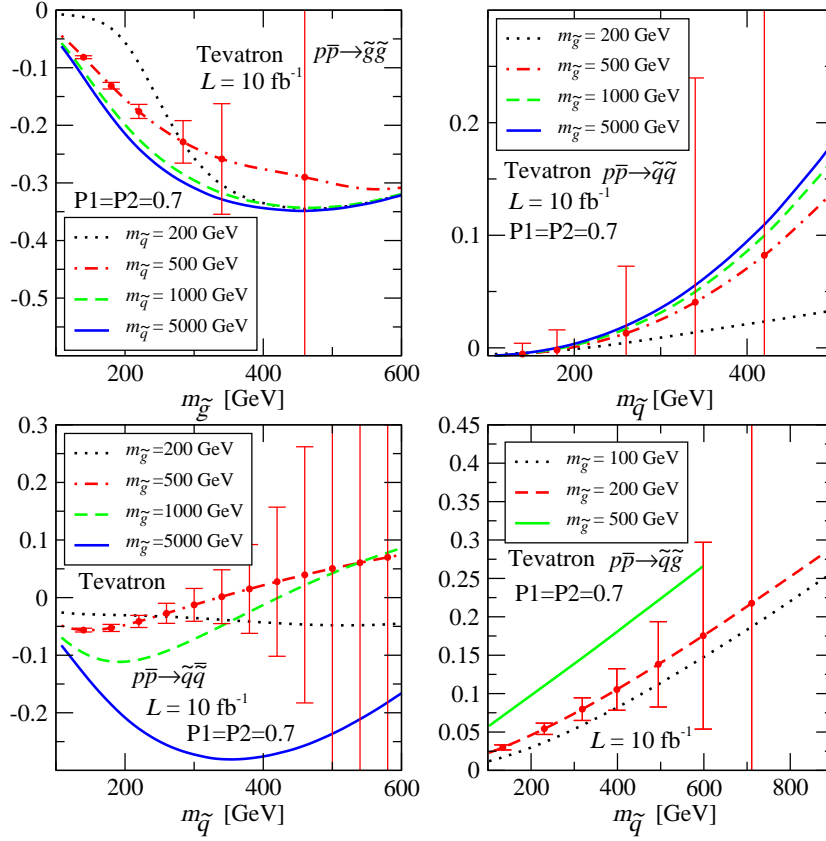


Figure 14: Statistical error on the asymmetry for the Tevatron. We have assumed a polarisation of 70% and a total integrated luminosity of 10 fb^{-1} .

and for a small deviation we get for δA :

$$\delta A^2 = \frac{4}{P_1^2 P_2^2} \frac{\Delta N_+^2 N_-^2 + \Delta N_-^2 N_+^2 - 2\Delta N_+ \Delta N_- N_+ N_-}{(N_+ + N_-)^2}.$$

The expectation value of this expression gives ΔA^2 :

$$\Delta A^2 = \langle \delta A^2 \rangle = \frac{4}{P_1^2 P_2^2} \frac{\langle \Delta N_+ \rangle^2 N_-^2 + \langle \Delta N_- \rangle^2 N_+^2}{(N_+ + N_-)^2}. \quad (43)$$

The final result for the statistical error of the asymmetry is obtained by inserting the deviation $\Delta N_{+/-}$ and expressing the result as a function of the asymmetry A and $N = N_+ + N_-$:

$$\Delta A^2 = \frac{4(N_+ N_-)}{N^2 P_1^2 P_2^2} = \frac{1}{N P_1^2 P_2^2} - \frac{A^2}{N^2}. \quad (44)$$

The expected statistical errors are collected in Figures 13-15.

For all three collider scenarios, the statistical errors grow with increasing sparticle masses such that statistically significant measurements are especially possible for low masses.

At RHIC the situation is quite favourable for $m_{\tilde{g}/\tilde{q}} \lesssim 75 \text{ GeV}$, except in squark-squark production. This process is a pure gluino t -channel exchange which is suppressed by the gluino mass.

At Tevatron, with a total integrated luminosity of 10 fb^{-1} , the statistical error starts getting important in the region $m_{\tilde{g}/\tilde{q}} \approx 350 \text{ GeV}$; the exception is squark-squark production where the statistical error is

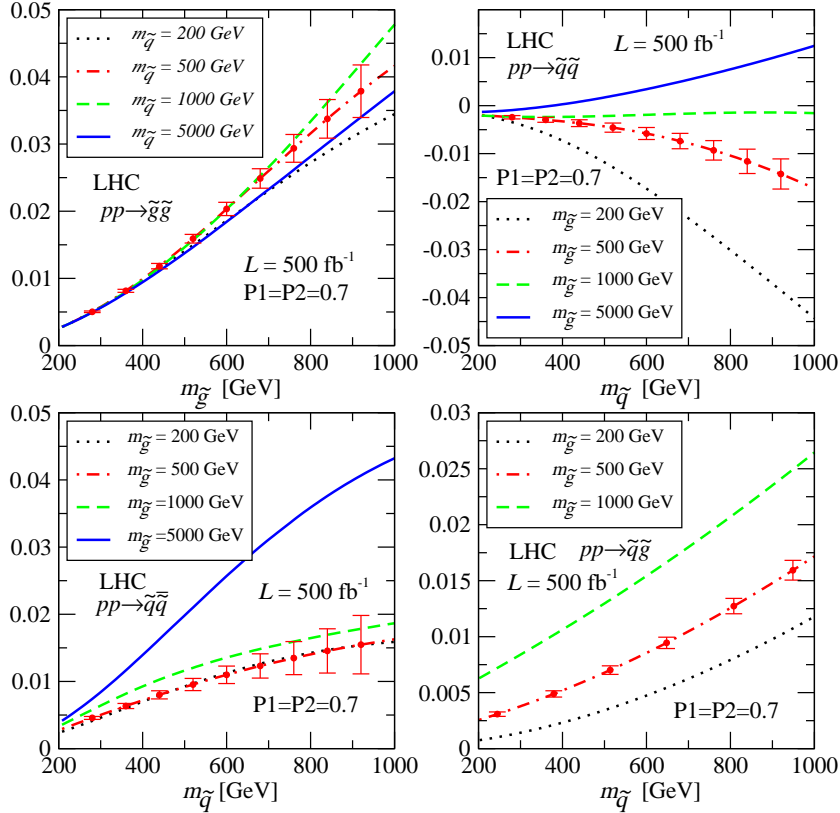


Figure 15: Statistical error on the asymmetry for the LHC. We have assumed a polarisation of 70% and a total integrated luminosity of 500 fb^{-1} .

larger than the asymmetry everywhere. At Tevatron, squark-squark production is particularly suppressed because the quark-quark luminosity is lower at a proton-antiproton collider than at a proton-proton collider.

At LHC, with a total integrated luminosity of 500 fb^{-1} , all channels (with the exception of squark-squark production with large gluino mass) display only moderate errors even up to sparticle masses of 1000 GeV. Therefore a measurement of spin asymmetries at LHC would be especially interesting, despite their apparent smallness.

In a realistic measurement it will be very difficult to distinguish between squark-antisquark and squark-squark final states and both might have to be summed over. The summed cross sections are mostly dominated by squark-antisquark final states, and the combined asymmetry would be of similar magnitude as the squark-antisquark asymmetry [39].

4 Transverse Momentum and Rapidity Spectra

In the previous section, we have established measurable spin asymmetries in inclusive squark and gluino production for a wide range of sparticle masses. In a measurement, one is however often not able to detect particles over the fully inclusive final state phase space but only in restricted ranges in the final state transverse momentum and rapidity. It is therefore important to study the dependence of the cross sections and asymmetries on the sparticle rapidity and transverse momentum.

The transverse momentum distribution of unpolarized and polarized cross sections are displayed in Figure 16. We observe that the majority of the sparticles are produced with sizable transverse momentum of about $(0.2 \dots 0.5)m_{\tilde{q}/\tilde{g}}$. Moreover, for almost all final states, we observe that the transverse momentum

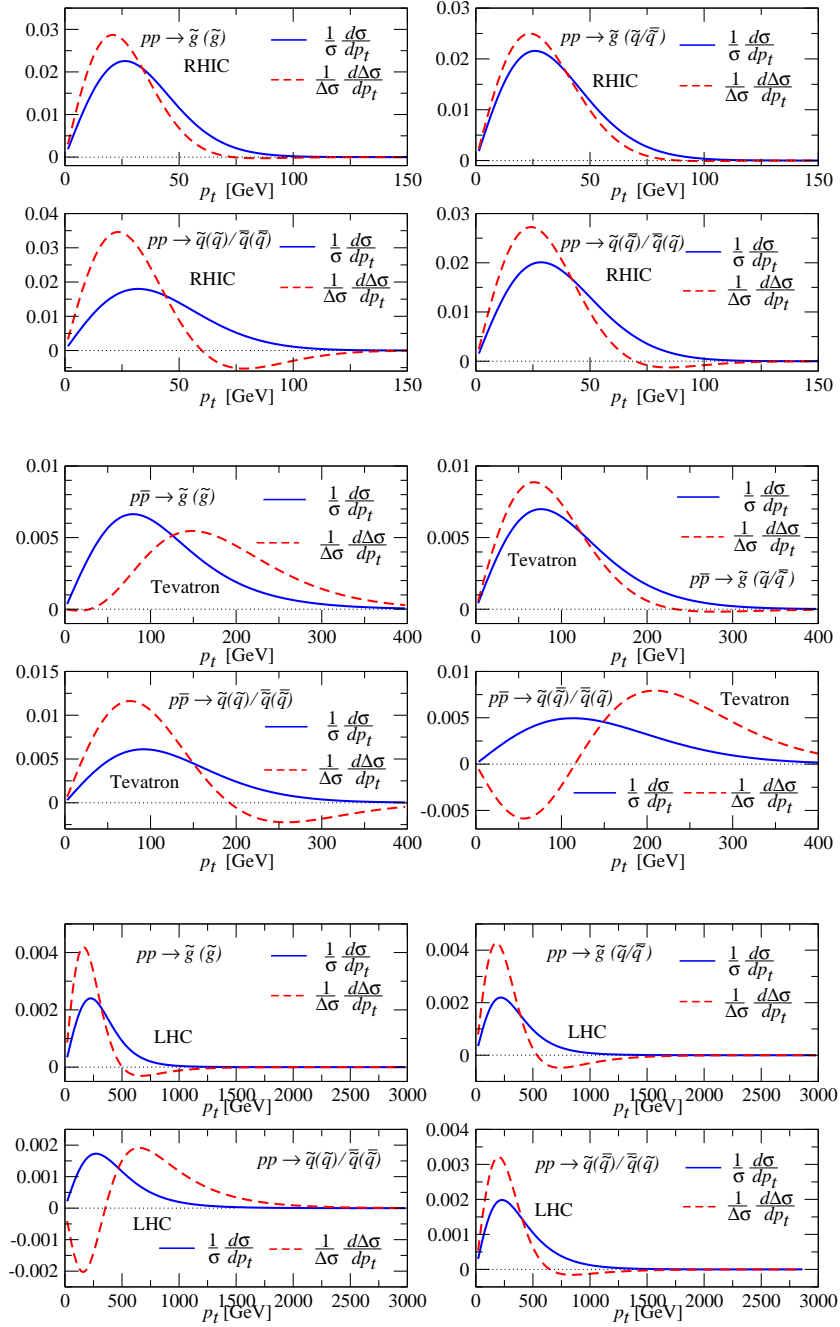


Figure 16: Normalised transverse momentum distribution for the three colliders LHC, Tevatron and RHIC. The mass parameters are for the LHC ($\sqrt{S} = 14$ TeV) $m_{\tilde{g}} = 500$ GeV, $m_{\tilde{q}} = 600$ GeV, for the Tevatron ($\sqrt{S} = 1.96$ TeV) $m_{\tilde{g}} = 200$ GeV, $m_{\tilde{q}} = 280$ GeV and for the RHIC ($\sqrt{S} = 500$ GeV) $m_{\tilde{g}} = 80$ GeV, $m_{\tilde{q}} = 100$ GeV.

distribution of unpolarized and polarized cross sections differ substantially. At the LHC, all polarized distributions change their sign between small and large transverse momenta. A similar feature is observed in some distributions at RHIC and the Tevatron. This behaviour reflects in part the structure of the polarized matrix elements, but also the form of the polarized parton distribution functions.

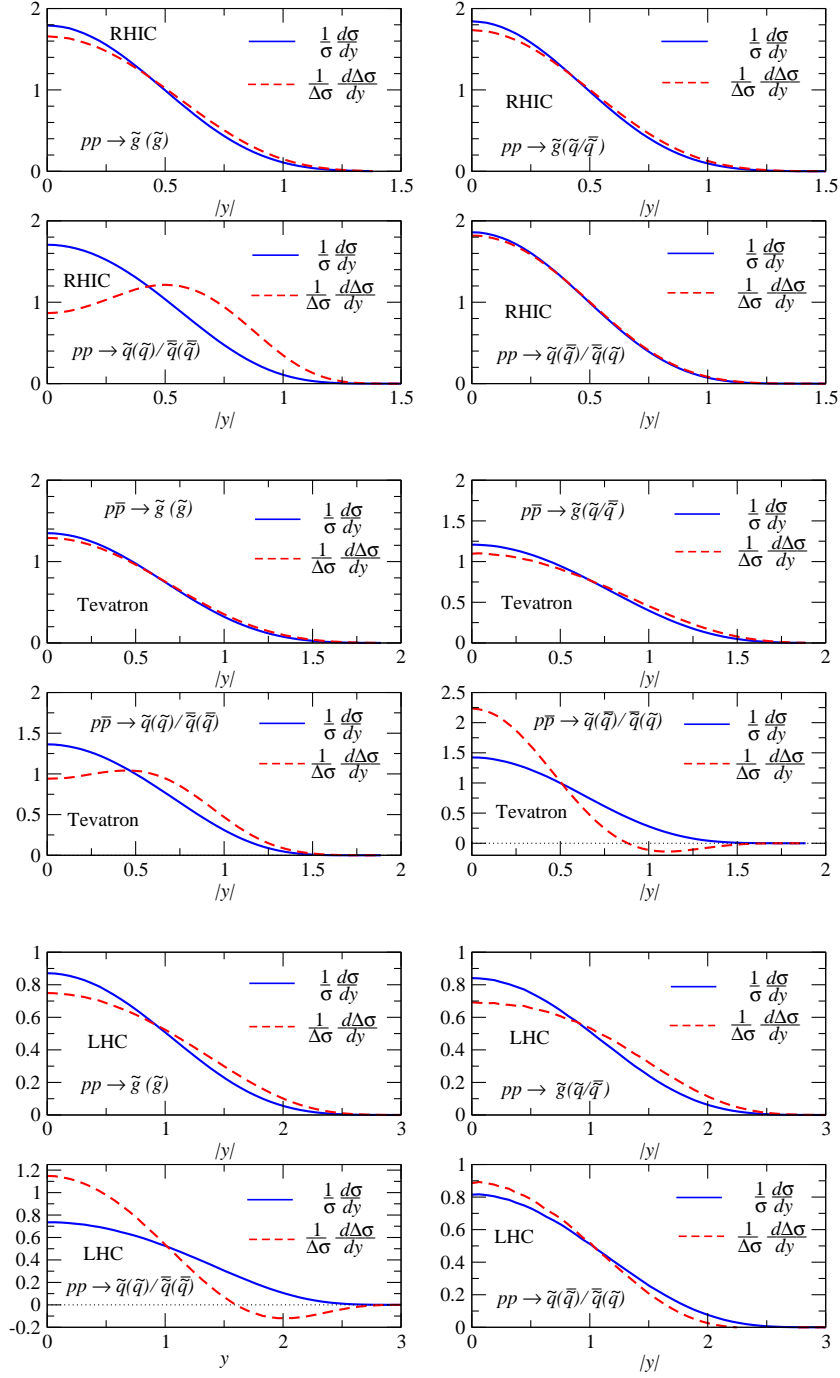


Figure 17: Normalised rapidity distributions for the three colliders LHC, Tevatron and RHIC. The mass parameters are for the LHC ($\sqrt{S} = 14$ TeV) $m_{\tilde{g}} = 500$ GeV, $m_{\tilde{q}} = 600$ GeV, for the Tevatron ($\sqrt{S} = 1.96$ TeV) $m_{\tilde{g}} = 200$ GeV, $m_{\tilde{q}} = 280$ GeV and for the RHIC ($\sqrt{S} = 500$ GeV) $m_{\tilde{g}} = 80$ GeV, $m_{\tilde{q}} = 100$ GeV.

At large transverse momenta, most polarized distributions fall off slower than their unpolarized counterparts. The explanation for this feature lies in the ratio between polarized and unpolarized parton distributions which increases towards larger values of x , corresponding to large values of the transverse

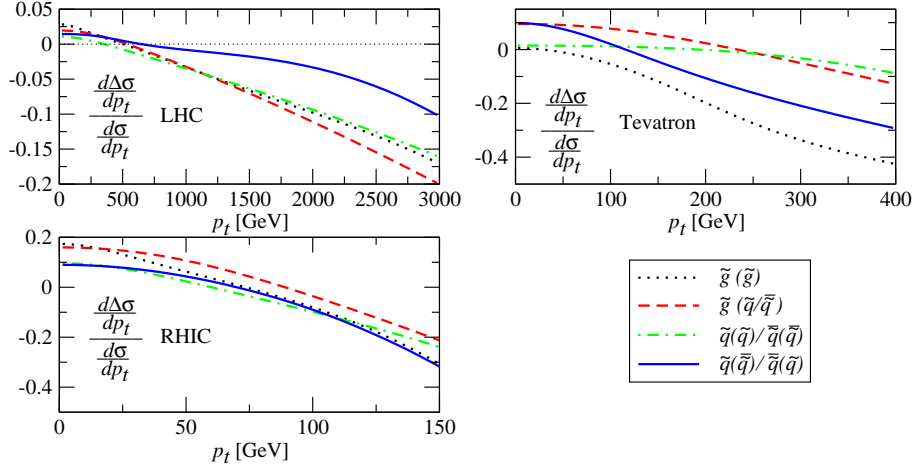


Figure 18: Asymmetry in the transverse momentum distribution for the three colliders LHC, Tevatron and RHIC. The mass parameters are for the LHC ($\sqrt{S} = 14$ TeV) $m_{\tilde{g}} = 500$ GeV, $m_{\tilde{q}} = 600$ GeV, for the Tevatron ($\sqrt{S} = 1.96$ TeV) $m_{\tilde{g}} = 200$ GeV, $m_{\tilde{q}} = 280$ GeV and for the RHIC ($\sqrt{S} = 500$ GeV) $m_{\tilde{g}} = 80$ GeV, $m_{\tilde{q}} = 100$ GeV.

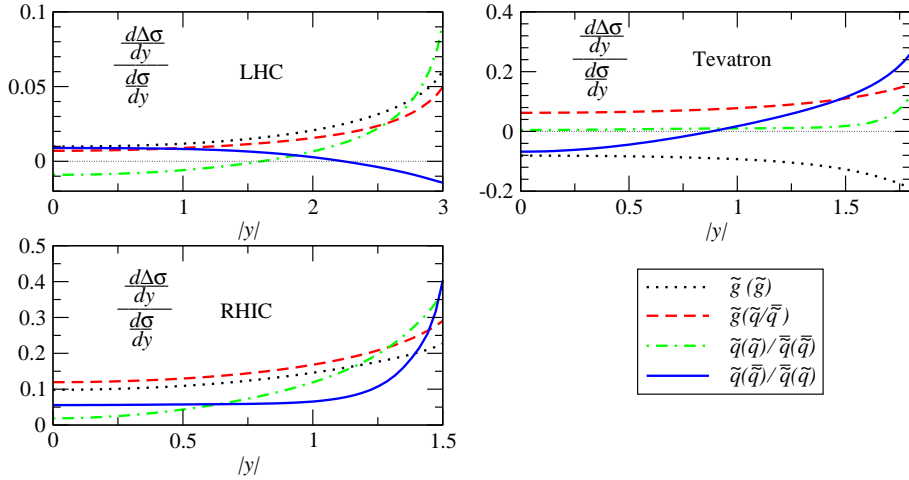


Figure 19: Asymmetry in the rapidity distribution for the three colliders LHC, Tevatron and RHIC. The mass parameters are for the LHC ($\sqrt{S} = 14$ TeV) $m_{\tilde{g}} = 500$ GeV, $m_{\tilde{q}} = 600$ GeV, for the Tevatron ($\sqrt{S} = 1.96$ TeV) $m_{\tilde{g}} = 200$ GeV, $m_{\tilde{q}} = 280$ GeV and for the RHIC ($\sqrt{S} = 500$ GeV) $m_{\tilde{g}} = 80$ GeV, $m_{\tilde{q}} = 100$ GeV.

momentum.

The rapidity distributions, Figure 17, are more uniform than the transverse momentum distributions. Most polarized distributions follow their unpolarized counterparts rather closely, showing in general a slower decrease towards larger rapidities.

The features of polarized and unpolarized transverse momentum and rapidity distributions become particularly visible in corresponding asymmetries, Figures 18 and 19. It can be seen that the transverse momentum spectrum of the spin asymmetry increases towards larger transverse momenta for all colliders and all final states. Several spectra display a zero. On the contrary, the rapidity dependence of the spin asymmetries is rather flat, especially in the experimentally most relevant central rapidity region.

5 Conclusions and Outlook

In this paper, we have studied spin asymmetries in squark and gluino production at polarized hadron colliders to leading order in QCD. We consider three scenarios, the currently operational polarized proton-proton collider RHIC and hypothetical polarized versions of the Tevatron and the LHC. For all three colliders, we find sizable spin asymmetries. Assuming the design luminosities and beam polarization of 70%, the asymmetries are statistically measurable for sparticle masses up to 75 GeV at RHIC, 350 GeV at the Tevatron and well above 1 TeV at LHC, provided experimental systematic uncertainties on them can be kept under control.

If supersymmetry is realized in nature, one would expect to see visible signatures of squarks and gluinos already in unpolarized hadronic collisions at the Tevatron or the LHC, depending on the particle masses. A subsequent measurement of spin asymmetries at potential polarized versions of these colliders could be vital to give detailed insights into the new physics and may distinguish between different supersymmetric models (or any other new physics idea). For instance, if (heavy) quarks and related squarks have similar masses and therefore similar production rates, the corresponding asymmetries are different. An asymmetry measurement could thus exclude a light bottom squark effectively⁵ or distinguish between a heavy fourth generation quark and a supersymmetric particle. It would also be quite significant if the sparticle masses are quite different from each other. For instance, as shown in the text, spin asymmetries in squark-antisquark production could be used to infer the gluino mass, even if direct gluino observation is beyond the kinematical reach of the collider. Apart from the additional information it provides, the spin asymmetry can also be measured with much less uncertainty than cross sections. As explained in the text, spin asymmetries are insensitive to absolute normalisation, which turns out to be a serious challenge at hadron colliders. We expect to have detailed knowledge of the required polarized parton distributions after measurements at RHIC and COMPASS have been completed. Our results contribute to making a physics case for a new polarized hadron collider at energies above RHIC or for an upgrade of an existing and planned high energy colliders to polarized hadrons.

There are further phenomenological applications. One particular aspect of using polarized initial states is that they offer the possibility to obtain event samples enriched either in L - or R -squarks which can not be discriminated at unpolarized hadron colliders.

A precise study of spin asymmetries in squark and gluino production would not only require an improved understanding of the spin-dependent parton distributions, but also the inclusion of next-to-leading order corrections to the partonic scattering processes. These are available for unpolarized squark and gluino production [26]. The calculation of the spin-dependent NLO corrections would resemble the NLO calculation of heavy quark production at polarized hadron colliders, which was completed some time ago [40]. In fact, as pointed out already in [40], the NLO corrections to the polarized cross section for $gg \rightarrow \tilde{g}\tilde{g}$ could already be obtained from the results on spin-dependent heavy quark production.

One possible environment to study polarized partonic scattering processes would be photon-photon interactions at a future linear collider [19], either realized by tagging onto bremsstrahlung photons or with a dedicated photon-photon programme using high energy photon beams generated by laser backscattering. In both options, the photon beams would be polarized. The polarized cross sections for squark and gluino production in direct and resolved photon interactions can be readily obtained from the formulae presented here. The polarized parton distributions in the photon are at present completely unconstrained by experimental data, theoretical models for them exist and put upper and lower boundaries on their magnitude [41]. Knowledge on them could furthermore be improved by studying spin asymmetries in standard model reactions in photon-photon collisions.

Acknowledgements

We would like to thank Philip Ratcliffe for pointing our attention to [23] and for useful discussions. This work was supported by the Swiss National Funds (SNF) under contract 200021-101874.

⁵As mentioned previously, this possibility is presumably already excluded.

References

- [1] D. Adams *et al.* [Spin Muon Collaboration (SMC)], Phys. Rev. D **56** (1997) 5330 [hep-ex/9702005]; B. Adeva [SMC Collaboration], Phys. Rev. D **70** (2004) 012002 [hep-ex/0402010].
- [2] P. L. Anthony *et al.* [E155 Collaboration], Phys. Lett. B **493** (2000) 19 [hep-ph/0007248].
- [3] K. Ackerstaff *et al.* [HERMES Collaboration], Phys. Lett. B **464** (1999) 123 [hep-ex/9906035]; A. Airapetian *et al.* [HERMES Collaboration], Phys. Rev. Lett. **92** (2004) 012005 [hep-ex/0307064].
- [4] X. Zheng *et al.* [Jefferson Lab Hall A Collaboration], Phys. Rev. Lett. **92** (2004) 012004 [nucl-ex/0308011].
- [5] M. D. Leberig [COMPASS Collaboration], Acta Phys. Polon. B **33** (2002) 3707 [hep-ex/0209047].
- [6] G. Bunce, N. Saito, J. Soffer and W. Vogelsang, Ann. Rev. Nucl. Part. Sci. **50** (2000) 525 [hep-ph/0007218].
- [7] M. Hirai, S. Kumano and N. Saito [Asymmetry Analysis Collaboration], Phys. Rev. D **69** (2004) 054021 [hep-ph/0312112].
- [8] J. Blümlein and H. Böttcher, Nucl. Phys. B **636** (2002) 225 [hep-ph/0203155].
- [9] M. Glück, E. Reya, M. Stratmann and W. Vogelsang, Phys. Rev. D **63** (2001) 094005 [hep-ph/0011215].
- [10] M. Glück, E. Reya, M. Stratmann and W. Vogelsang, Phys. Rev. D **53** (1996) 4775 [hep-ph/9508347].
- [11] T. Gehrmann and W. J. Stirling, Phys. Rev. D **53** (1996) 6100 [hep-ph/9512406].
- [12] G. Altarelli, R. D. Ball, S. Forte and G. Ridolfi, Nucl. Phys. B **496** (1997) 337 [hep-ph/9701289].
- [13] P. Taxil and J. M. Virey, Phys. Rev. D **55** (1997) 4480 [hep-ph/9607390].
- [14] J. M. Virey, Eur. Phys. J. C **8** (1999) 283 [hep-ph/9809439].
- [15] P. Taxil, E. Tugcu and J. M. Virey, Eur. Phys. J. C **24** (2002) 149 [hep-ph/0111242].
- [16] H. P. Nilles, Phys. Rept. **110** (1984) 1;
H. E. Haber and G. L. Kane, Phys. Rept. **117** (1985) 75.
- [17] G. Moortgat-Pick, A. Bartl, H. Fraas and W. Majerotto, Eur. Phys. J. C **18** (2000) 379 [hep-ph/0007222];
C. Blochinger, H. Fraas, G. Moortgat-Pick and W. Porod, Eur. Phys. J. C **24** (2002) 297 [hep-ph/0201282].
- [18] D. K. Ghosh and S. Moretti, Phys. Rev. D **66** (2002) 035004 [hep-ph/0112288].
- [19] R.D. Heuer, D.J. Miller, F. Richard and P.M. Zerwas (Eds.), “TESLA Technical Design Report Part III: Physics at an e^+e^- Linear Collider”, DESY-report 2001-011 [hep-ph/0106315].
- [20] S. Berge, M. Klasen and Y. Umeda, Phys. Rev. D **63** (2001) 035003 [hep-ph/0008081].
- [21] S. Berge and M. Klasen, Phys. Rev. D **66** (2002) 115014 [hep-ph/0208212]; Eur. Phys. J. C **30** (2003) 123 [hep-ph/0303032].
- [22] K. Desch, J. Kalinowski, G. Moortgat-Pick, M. M. Nojiri and G. Polesello, JHEP **0402** (2004) 035 [hep-ph/0312069].
- [23] N.S. Craigie, K. Hidaka and P. Ratcliffe, Phys. Lett. B **129** (1983) 310.
- [24] P. Chiappetta, J. Soffer and P. Taxil, Phys. Lett. B **162** (1985) 192.

- [25] G. L. Kane and J. P. Leveille, Phys. Lett. B **112** (1982) 227;
P. R. Harrison and C. H. Llewellyn Smith, Nucl. Phys. B **213** (1983) 223 [Erratum B **223** (1983) 542];
E. Reya and D. P. Roy, Phys. Rev. D **32** (1985) 645;
S. Dawson, E. Eichten and C. Quigg, Phys. Rev. D **31** (1985) 1581;
H. Baer and X. Tata, Phys. Lett. B **160** (1985) 159.
- [26] W. Beenakker, R. Höpker, M. Spira and P. M. Zerwas, Phys. Rev. Lett. **74** (1995) 2905 [hep-ph/9412272]; Z. Phys. C **69** (1995) 163 [hep-ph/9505416]; Nucl. Phys. B **492** (1997) 51 [hep-ph/9610490].
- [27] B. Abbott *et al.* [D0 Collaboration], Phys. Rev. Lett. **83** (1999) 4937 [hep-ex/9902013];
T. Affolder *et al.* [CDF Collaboration], Phys. Rev. Lett. **88** (2002) 041801 [hep-ex/0106001].
- [28] E.L. Berger, B.W. Harris, D.E. Kaplan, Z. Sullivan, T.M.P. Tait and C.E.M. Wagner, Phys. Rev. Lett. **86** (2001) 4231 [hep-ph/0012001].
- [29] P. Janot, Phys. Lett. B **564** (2003) 183 [hep-ph/0302076]; Phys. Lett. B **594** (2004) 23 [hep-ph/0403157].
- [30] M. Cacciari and P. Nason, Phys. Rev. Lett. **89** (2002) 122003 [hep-ph/0204025].
- [31] M. Cacciari, S. Frixione, M. L. Mangano, P. Nason and G. Ridolfi, JHEP **0407** (2004) 033 [hep-ph/0312132].
- [32] E.L. Berger, P.M. Nadolsky, F.I. Olness and J. Pumplin, hep-ph/0406143.
- [33] J. Rosiek, Phys. Rev. D **41** (1990) 3464; hep-ph/9511250.
- [34] A. Denner, H. Eck, O. Hahn and J. Küblbeck, Nucl. Phys. B **387** (1992) 467.
- [35] W. Beenakker, M. Krämer, T. Plehn, M. Spira and P. M. Zerwas, Nucl. Phys. B **515** (1998) 3 [hep-ph/9710451].
- [36] M. Glück, E. Reya and A. Vogt, Eur. Phys. J. C **5** (1998) 461 [hep-ph/9806404].
- [37] M. Glück, E. Reya and M. Stratmann, Nucl. Phys. B **422** (1994) 37.
- [38] M. Glück, E. Reya and A. Vogt, Z. Phys. C **53** (1992) 127.
- [39] D. Maître, Diplomarbeit, ETH Zürich, 2004.
- [40] I. Bojak and M. Stratmann, Phys. Rev. D **67** (2003) 034010 [hep-ph/0112276].
- [41] M. Stratmann and W. Vogelsang, Phys. Lett. B **386** (1996) 370 [hep-ph/9606346].